Materials Advances

PAPER

Check for updates

Ugi reaction-enabled one-step multifunctionalization of biocatalytic VLPs for multimodal therapeutics

Andrea Dorado-Baeza, Daniel Pliego Sosa, [iD] Ana G. Rodríguez-Hernández, Prakhar Sengar, Rafael Vazquez-Duhalt [iD] and Kanchan Chauhan [iD] *

Multimodal nanoplatforms hold great potential in cancer therapy, but their clinical translation is limited by complex, multi-step synthesis. While protein nanocages provide a homogeneous and multifunctional scaffold, their complex architecture restricts compatibility with many chemical reactions. Here, we report the first successful use of the Ugi four-component reaction (Ugi-4CR) for one-step multifunctionalization of biocatalytic P22 encapsulating cytochrome P450 (CYP). Functionalization included glucose oxidase (GOx) for cascade enzymatic prodrug activation and glucosamine (GA) as a targeting ligand. A parallel labeling of protein with dye, indocyanine green (ICG), for near infrared (NIR) imaging and NIR-mediated phototherapy was also performed. The reaction showed high reproducibility with similar degrees of conjugation of GOx and ICG in each reaction. Enzymatic cascade kinetic analysis showed ∼3-fold improved catalytic efficiency of Ugi-produced nanoreactors compared to conventional carbodiimide coupling, while maximum velocity was reduced by ∼2-fold. The glucose-triggered activation of the prodrug using engineered nanoreactors in the absence and presence of NIR revealed a potential for synergistic chemo-photothermal therapy. Additionally, *in vitro* studies exhibited improved cellular uptake of targeted nanoreactors. Overall, the results confirm the intact functional integration of all the integrated components under Ugi conditions and hint at site-selective modification on the VLP surface. This work shows that the Ugi-4CR has potential for one-step multifunctionalization of protein nanocages to develop comprehensive therapeutic modalities, offering faster and efficient alternatives to tedious multi-step functionalization strategies.

1. Introduction

Cancer is still a major health issue in the world.[1] Despite advances in therapy, the inherent complexity, heterogeneity, and adaptability of tumors continue to challenge effective cancer treatment. Monotherapies, which employ a single therapeutic approach, often fail to eliminate tumors.[2,3] In this context, nanomedicine has emerged as a powerful tool offering targeted delivery, improved therapeutic efficacy, and reduced systemic toxicity.[4] This has paved the way for innovative strategies involving patient stratification, rational drug selection, combination therapies, and immunomodulation.[5]

Multimodal synergistic therapy combining multiple therapeutic agents or strategies within a single platform, has recently gained attention due to its potential to overcome resistance and enhance therapeutic response. Such platforms typically integrate a nanocarrier, surface modifiers, and encapsulated functional agents, forming multifunctional nanostructures capable of simultaneous diagnosis and treatment.[3] Among various nanocarriers, protein nanocages like virus-like particles (VLPs) offer a versatile and biocompatible scaffold due to their monodispersity, multivalency for surface modifications, genetic modifiability, and ability to encapsulate diverse cargo.[6,7] However, their functionalization remains challenging, primarily due to harsh conditions that can compromise nanoparticle stability and bioactivity if used as enzyme carriers. There are only a few reactions, like esterification, amidation, aryl diazonium reactions, *etc.*, that involve mild reaction conditions. However, they have their advantages and limitations (Table 1). Moreover, most surface conjugation strategies for multifunctionalization often involve tedious multi-step protocols, significantly reducing the scalability, reproducibility, and overall yield.[8]

In this context, isocyanide based multicomponent reactions (MCRs) offer an attractive alternative. These reactions allow the one-pot assembly of complex molecules from simple starting materials, promoting higher yields, faster synthesis, and greener

Centro de Nanociencias y Nanotecnologia, Universidad Nacional Autonoma de Mexico, Km 107 carretera, Tijuana-Ensenada, Baja California 22860, Mexico.
E-mail: kanchan_chauhan@ens.cnyn.unam.mx

Table 1 Common bioconjugation strategies at ambient conditions and aqueous medium[7,20,21]

Reaction type	Target residues	Selectivity	Advantages	Disadvantages
Amide bond (EDC/NHS) (NHS-ester)	Carboxylic acid + amine / Amine	Low	Simple, common	Non-specific; potential protein crosslinking, Low shelf life of NHS-ester
Thiol-maleimide	Cysteine	High	Site-specific, stable thioether bond	Hydrolytic instability of maleimide, cysteine availability issue
Aldehyde-amine	N-terminal/lysine	Moderate	Reductive amination stabilizes product	Reversible Schiff base formation if unreduced
Diazonium coupling	Tyrosine	Moderate	Aromatic selectivity possible	Harsh conditions, less common reagents
Disulfide bonding	Cysteine	Moderate	Reversible, useful for redox systems	Unstable in reducing environments, cysteine availability issue

chemistry principles.[9] Among MCRs, the Ugi four-component reaction (Ugi-4CR), discovered by Ivar Karl Ugi in 1959, stands out for its versatility. It involves the combination of an amine, an aldehyde, an isocyanide, and a carboxylic acid to yield α-acetoamido carboxamides, enabling multiple C–C and C–N bonds *via* bis-amide formation in a single step.[10,11] While Ugi has been extensively used in peptide chemistry, its exploration in protein conjugation chemistry is only a handful. Rezai *et al.* reported the successful aqueous-phase Ugi-4CR-based immobilization of glucose oxidase (GOx) and glucoamylase on silver dendrites, offering an efficient and environmentally benign method for enzyme attachment with retained bioactivity.[8] Recently, site-selective conjugation of native trastuzumab using Ugi-3CR-4centered reaction further demonstrated the potential of MCRs for antibody functionalization.[12] However, its utility in modifying complex protein nanostructures like VLPs remains largely unexplored.

In our group, VLPs have been successfully used to encapsulate therapeutic enzymes such as *Bacillus megaterium*-derived cytochrome P450 (CYP), a monooxygenase capable of catalyzing epoxidation and hydroxylation reactions using hydrogen peroxide.[13–17] Most chemotherapeutic drugs like tamoxifen and resveratrol are prodrugs that require metabolic activation by CYP to show anti-cancerous effect, indicating its value in enzyme prodrug therapy of cancer.[18] Sánchez-Sánchez *et al.* encapsulated CYP in Cowpea Chlorotic Mottle Virus (CCMV) and bacteriophage P22 VLPs to demonstrate efficient prodrug conversion.[13] P22 encapsulating CYP (P22CYP) was further engineered to co-deliver estradiol, and the photosensitizer protoporphyrin IX (PpIX), achieving a multimodal nanoreactor for ER+ breast cancer treatment through combined prodrug activation and photodynamic therapy.[16] Recently, dual enzyme nanoreactors have also been explored by co-immobilizing another enzyme, glucose oxidase (GOx), with CYP. This system can initiate an enzymatic cascade reaction in the presence of glucose, which is rich in the tumor microenvironment (TME). The immobilized glucose oxidase (GOx) catalyzes the consumption of glucose, which serves as the primary energy source for cancer cells, simultaneously producing hydrogen peroxide that acts as the terminal electron acceptor in CYP-mediated catalytic reactions.[17,19]

Herein, the optimization of a Ugi-4CR-based strategy to enable the simultaneous multifunctionalization of P22CYP with distinct functional components: GOx as a catalytic cascade enzyme, and 2-glucosamine (GA) as a targeting ligand is reported. A parallel labeling with indocyanine green (ICG) as a photosensitizer was also performed during the reaction. This work aims to demonstrate the feasibility and efficiency of single-step Ugi-4CR for constructing biocompatible, multifunctional VLP-based nanoreactors with potential application in multimodal cancer therapeutics. Overall, this modular bioconjugation preserved enzyme activity and structural integrity of VLPs while making them a multimodal platform for the targeted quadruple therapy combining enzyme-prodrug, starvation, photodynamic, and photothermal therapies against breast cancer.

2. Results and discussion

Cancer heterogeneity remains a major challenge in therapy, and multimodal nanoplatforms offer a way to address it by integrating targeting, imaging, and therapeutic functions in a single system. Protein nanocages are promising scaffolds, but their complex architecture limits compatibility with many conjugation chemistries. Existing multimodal platforms often rely on multistep functionalization that is time-consuming, difficult to reproduce, and often compromise protein stability. Therefore, Ugi four-component reaction (Ugi-4CR) has been investigated as a one-step strategy to multifunctionalize P22 nanoreactors, enabling simultaneous enzymatic, targeting, imaging, and therapeutic capabilities.

To establish the feasibility of using the Ugi reaction, P22CYP was used as a nanocarrier to expand our previous work for multimodal cancer therapy.[16,19] It was obtained and successfully purified according to our previous reports.[14,15] After purification, P22-CYP was obtained with 110 encapsulated CYP molecules, confinement molarity of 3.29 mM, and internal occupancy of 29.9% [Section S1, SI]. The CYP enzyme kinetics were calculated, obtaining a K_M of 0.36 mM and V_{max} of 44 nmole min^{-1}, equivalent to the conversion of 1198 molecules of substrate per minute per nanoreactor [Section S2 in SI]. This confirmed the CYP activity of the nanoreactors using H_2O_2 as the final electron acceptor.

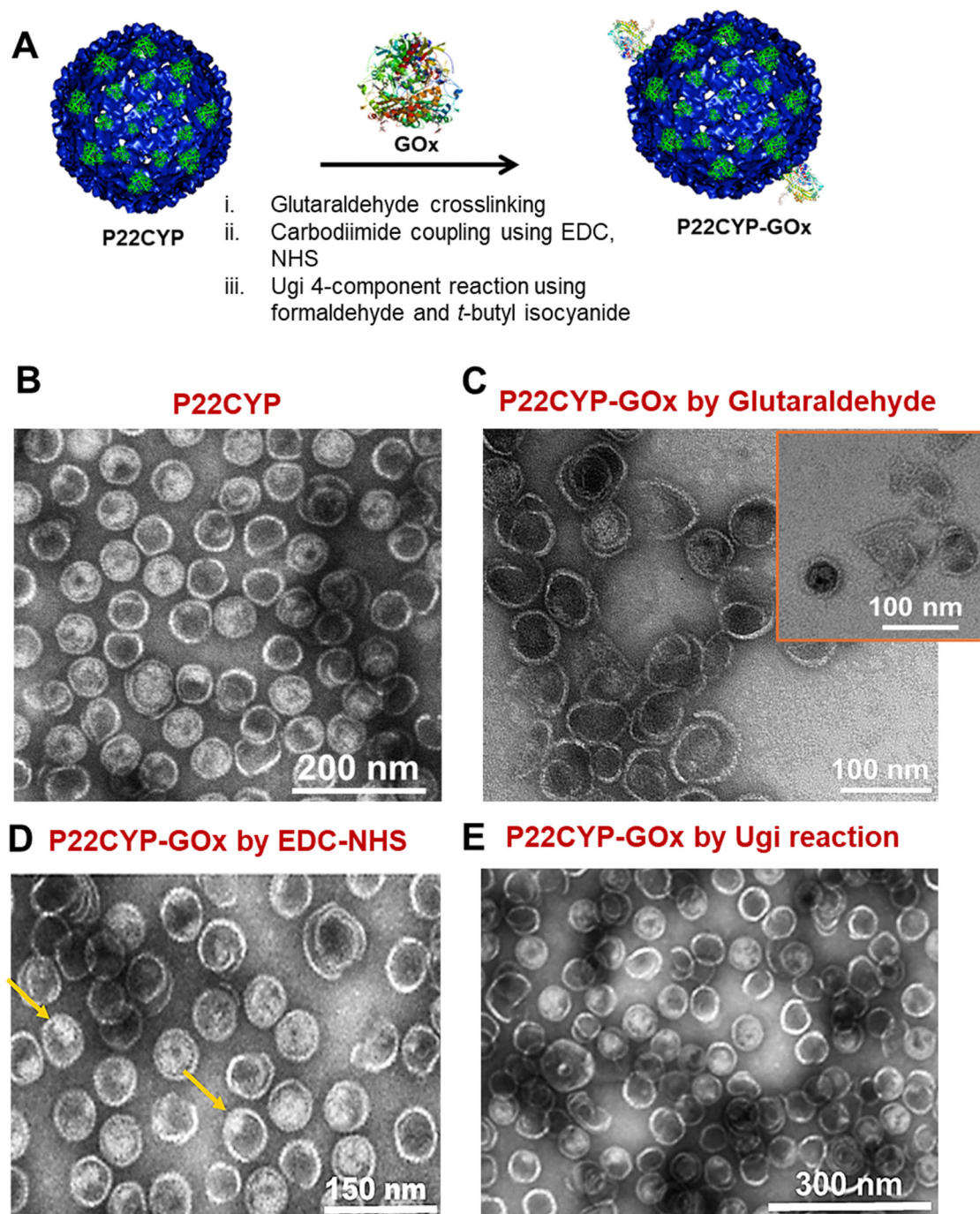Before multifunctionalization with different components, the performance of the Ugi reaction in enzyme conjugation

Fig. 1 Surface functionalization of P22CYP with GOx using three covalent modification strategies. (A) Schematic representation of P22CYP functionalization. (B) TEM image of native P22CYP showing uniform morphology. (C) P22CYP–GOx conjugates prepared using glutaraldehyde show distorted and aggregated particles. (D) EDC–NHS-mediated conjugates retain morphology. (E) Ugi-conjugated P22CYP–GOx also exhibits intact, well-dispersed VLPs.

was evaluated by using GOx to produce cascade nanoreactors. At this stage, conjugation by Ugi was also compared with two widely used covalent conjugation approaches for enzyme immobilization, glutaraldehyde (GHD) crosslinking, and EDC–NHS carbodiimide coupling (Fig. 1a). A 1 : 1 mass ratio of nanoreactors to GOx was used, as it was previously identified as optimal for maximizing cascade activity.[17] All the reactions were carried out

for 2 h at room temperature, and the product was obtained as a pellet after ultracentrifugation, which was resuspended and characterized. The reactions were compared in terms of conjugation efficiency, structural integrity, and compatibility with the P22CYP nanocage system.

Transmission electron microscopy (TEM) images reveal distinct structural differences among the modified particles.

Unmodified P22CYP displays uniformly spherical and well-dispersed particles with ∼60 nm diameter, serving as a control (Fig. 1b). Bigger aberrant structures and open capsids were similar to those reported by Zlotnic *et al.* due to the absence of scaffold protein and the coat protein polymerization.[22] P22CYP–GOx by glutaraldehyde crosslinking shows partially aggregated VLPs, with some loss of discrete morphology (Fig. 1c). The inset highlights distorted capsids, likely due to extensive crosslinking between amines on GOx and P22, resulting in interparticle crosslinking. On the other hand, P22CYP–GOx by EDC–NHS (Fig. 1d) and Ugi reaction (Fig. 1e) show well-dispersed, intact nanocages with minimal aggregation, suggesting structural preservation.

The biochemical compatibility of the Ugi reaction with the functional integrity of enzymes immobilized on protein nanocages was analyzed through enzymatic activity assays. The amount of immobilized GOx and the residual activity of CYP cargo within the P22 nanocage were measured (Fig. 2a). The amount of GOx immobilized on P22CYP nanocages was slightly higher in the Ugi reaction (5 μg mg^{-1} total protein) compared to EDC–NHS (2.8 μg mg^{-1} total protein), both significantly higher than the glutaraldehyde (GHD) crosslinking approach. Similarly, residual CYP activity was preserved best in EDC–NHS, closely followed by Ugi, with >90% activity recovery, while GHD resulted in the drastic loss of enzymatic activity, likely due to its extensive crosslinking, which can compromise protein structure.[23] GHD concentration is critical to preserve catalytic function. Studies have shown that a mild concentration of ∼5 mM is sufficient to saturate surface-exposed amines without disrupting the protein's tertiary structure, while exceeding 10 mM reduces enzymatic activity due to excessive crosslinking and conformational rigidity.[24–26] Therefore, 5 mM GHD was used for enzyme crosslinking, however, it seems to disrupt the VLP structure as well as reduce enzymatic activity significantly.
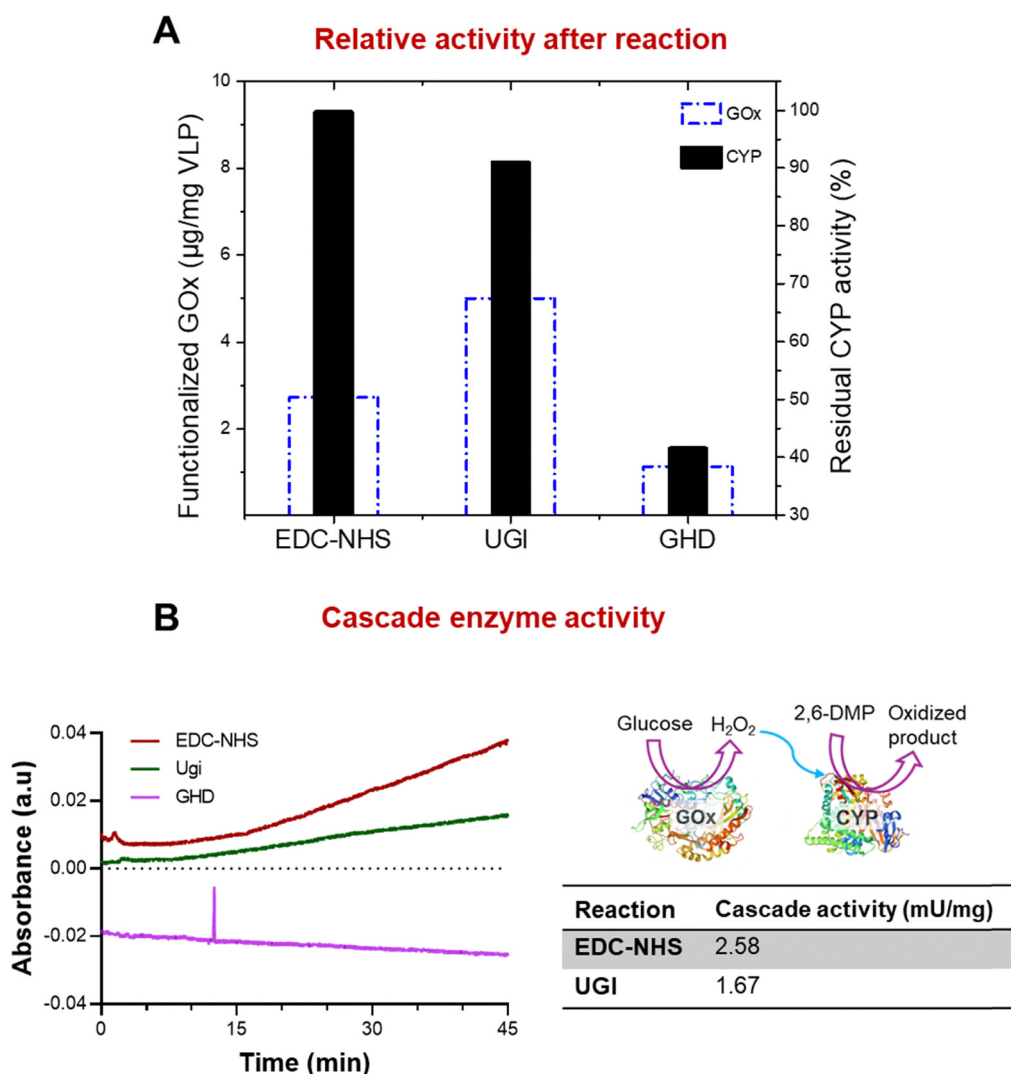

Reaction	Cascade activity (mU/mg)
EDC-NHS	2.58
UGI	1.67

Fig. 2 Evaluation of enzyme immobilization and catalytic performance of P22CYP–GOx nanoreactors functionalized by different conjugation strategies. (A) Quantification of immobilized GOx and residual CYP activity after each conjugation strategy. (B) Cascade enzyme activity assay to analyze 2,6-DMP transformation by *in situ* production of H$_2$O$_2$ in the presence of glucose. The schematic illustrates the cascade mechanism. The table indicates calculated specific activity (U mg^{-1} total protein).

More optimizations of GHD concentrations may improve the conjugation outcomes. Impressively, the Ugi reaction was comparable to carbodiimide coupling, preserving the VLPs' structure as well as enzyme function.

To determine whether both enzymes remained catalytically competent, an enzymatic cascade reaction where H_2O_2 generated by GOx drives CYP-mediated oxidation of 2,6-DMP was performed. The cascade activity, shown in Fig. 2b, was highest for EDC–NHS but remained appreciable in the Ugi reaction. While no meaningful cascade function was observed in the GHD reaction, again confirming its detrimental effect on protein function at 6 mM concentration.

After the successful immobilization of GOx under Ugi conditions, the subsequent multifunctionalization with additional components was optimized. In addition to P22CYP and GOx, the additional components were glucosamine (GA) for targeting ability and indocyanine green (ICG) as a photosensitizer. GA is a naturally occurring amino sugar that can potentially target cancer cells due to their elevated glucose uptake and increased expression of glucose transporters. Its structural similarity to glucose enables tumor cells to selectively internalize it, making it a valuable ligand for targeted drug delivery systems.[27,28] ICG is an FDA-approved near-infrared (NIR) dye used in cancer theranostics for its deep tissue penetration and low toxicity. Upon NIR irradiation, heat and reactive oxygen species (ROS) are generated, enabling photothermal (PT) and photodynamic therapy (PDT).[29,30] Together, these components enable a targeted multimodal nanoplatform that integrates enzyme prodrug therapy *via* cascade reactions, oxidative and starvation therapy through GOx activity, and near-infrared (NIR) imaging and phototherapy *via* ICG. However, it is important to evaluate the integrity of each component after multifunctionalization *via* Ugi reaction.

The multifunctionalization process was performed as shown in the schematic diagram (Fig. 3a). The UGI-based conjugation strategy, where amine-bearing glucosamine (targeting ligand), an aldehyde (formaldehyde), an isocyanide (*t*-butyl isocyanide), P22CYP, carboxylic acid groups rich GOx, and indocyanine green were combined under different reagent (formaldehyde and *t*-butyl isocyanide) concentrations (9 μM–8 mM) for 2 h. After the reaction, the mixture was washed three times through Amicon filtration (100 kDa cut off) to remove excess reagents and unbound GA and ICG from the reaction, and finally ultracentrifuged to remove free GOx. A visible change in pellet color (green color, red arrow) indicated successful conjugation.

TEM images of nanoreactors revealed a retained spherical morphology and monodispersity of P22CYP particles, suggesting structural integrity at even the highest concentration used. These results support that the Ugi reaction at variable reagent concentrations does not compromise VLP integrity.

Further, the nanoreactors were systematically evaluated for the effect of varying reagent concentrations and ionic strength on conjugation efficiency of GOx, CYP residual activity, and specific activity to determine optimal biocatalytic performance.

The functionalization efficiency of GOx, represented as bound GOx (%), as well was residual CYP activity was comparable across all conditions. The bound GOx percentage was slightly lowered with decreasing reagent concentration while CYP activity (%) was relatively stable at lower reagent concentrations (Fig. 4a). The highest CYP activity retention (~52%) was observed at 90 μM. The residual CYP activity when P22 was functionalized with only GOx through UGI reaction was ~93% (Fig. 2a), which was ~1.8 fold higher compared to multi component conjugation in the presence of different other elements. The higher degree of conjugation of different components on the VLP surface may limit the substrate diffusion to some extent, which might be the reason for lowered activity recovery. A similar behavior was also found when polyethylene glycol (PEG) was previously functionalized on the VLP surface.[16] These findings imply that Ugi-mediated conjugation retains enzymatic activity, preserving its functional integrity. Specific activity analysis further revealed complementary trends (Fig. 4b). GOx activity was in a similar range from 1.0 to 1.5 U mg^{-1}, while CYP activity remained within 5–6 mU mg^{-1} across all conditions.

The reproducibility of the reaction was analyzed with mild reagent concentrations varying from 9 μM to 2 mM by performing five sets of reactions. The odor of *t*-butyl isocyanide was very strong, especially in >2 mM concentrations, making it challenging to handle the reaction. The reaction required several washings through Amicon filtration to eliminate the odor, therefore, reactions with higher reagent concentration were not repeated. The data (Fig. 4a–c) is presented as the mean and standard deviation from multiple reactions. The low standard deviations obtained for GOx and CYP activity under these conditions reveal high reaction reproducibility with impressive consistency in conjugation (Fig. 4a and b). This is promising for scaling up production, as consistent surface functionalization is crucial in nanomaterials and bioconjugates. The GOx conjugation level doesn't increase with excess reagents, supporting the idea that only a subset of sites is reactive on protein surface, thereby, giving hints for reaction selectivity.

Sornay *et al.* performed multicomponent Ugi-4-component-3-reagent and Passerini reactions for bioconjugation on the antibody, trastuzumab.[12] The peptide mapping and native mass analysis demonstrated that under mild conditions, with equimolar aldehyde and isocyanide, the Ugi four-centered reaction predominates, particularly when neighboring amino (lysine) and carboxylate (aspartate/glutamate) residues are available in close proximity. Conversely, the Passerini reaction was favored by isolated carboxylate groups that lack nearby amines. It was also found that both reactions compete and occur in parallel. In our experimental system, the presence of an amine-containing glucosamine reagent at a large molar excess (1200) relative to P22, likely reduces the availability of isolated carboxylates, tipping the balance toward the Ugi pathway. Although, the formation of by-products from Passerini or other side reactions cannot be ruled out, the high reproducibility of the modifications under short reaction time (~2 h), mild temperature (18 °C), and presence of all four canonical components of the Ugi 4-component reaction support the Ugi pathway as the most likely. The previous work also showed the absence of inter-antibody crosslinking,
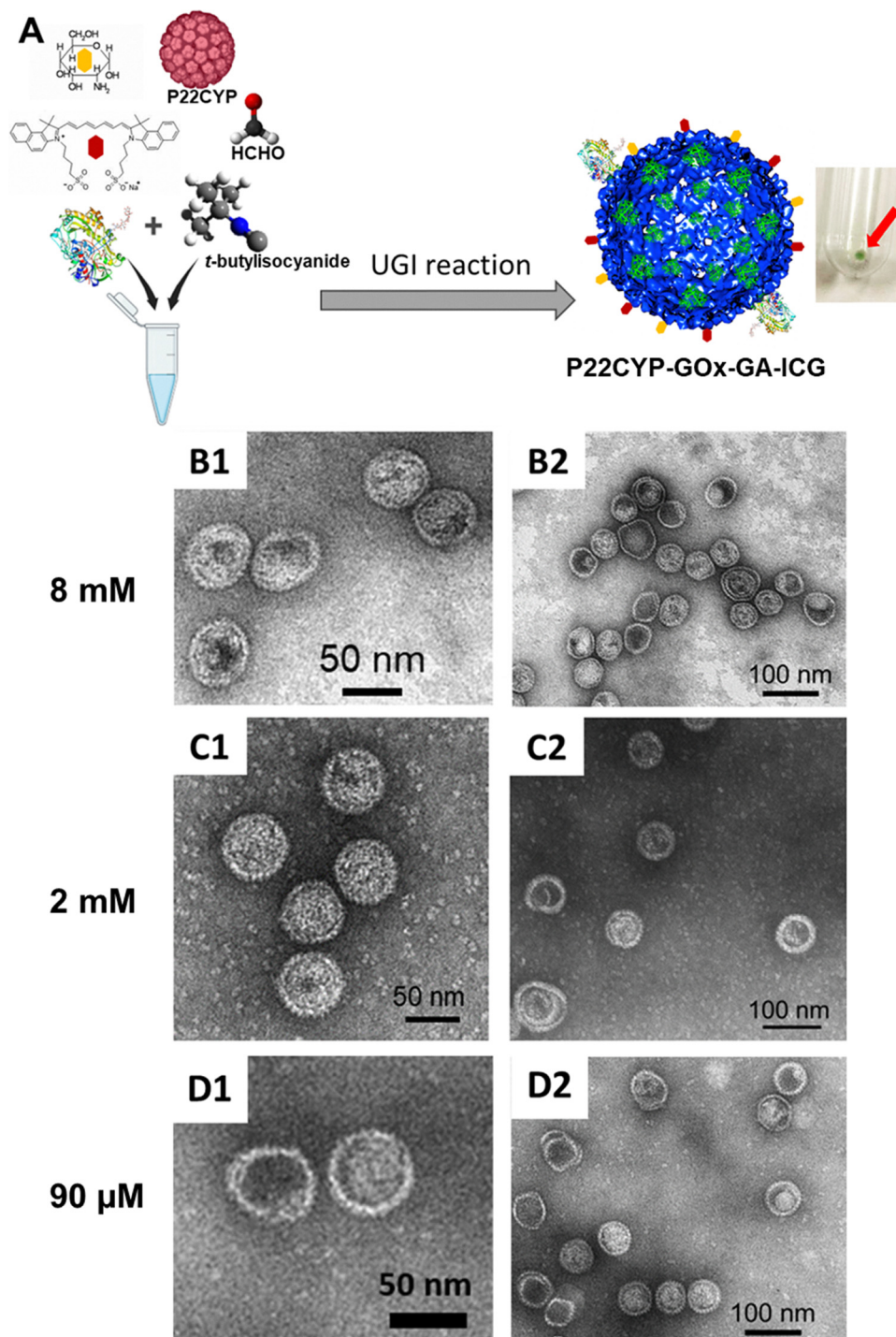
Fig. 3 Optimization of Ugi reaction on P22CYP nanoreactors at varying reagent (formaldehyde and *t*-butyl isocyanide) concentrations. (A) Schematic overview of the Ugi reaction on the surface of P22CYP. (B)–(D) Transmission electron microscopy (TEM) images of nanoreactors after Ugi modification under different reagent concentrations.

validated through circular dichroism analysis, supports intra-molecular site preference, likely due to steric hindrance preventing non-specific interactions between two protein molecules. In our study, the high reagent concentration did not cause any aggregation in VLPs, as evident by TEM analysis, indicating similar behavior. However, true site-selectivity and the reaction pathway (whether Ugi or Passerini or other side reaction) on more complex protein networks on VLPs would require further in-depth structural and analytical evidence. Importantly, isocyanide based multicomponent reaction on VLP surface was successful with preserved nanostructure and morphology.
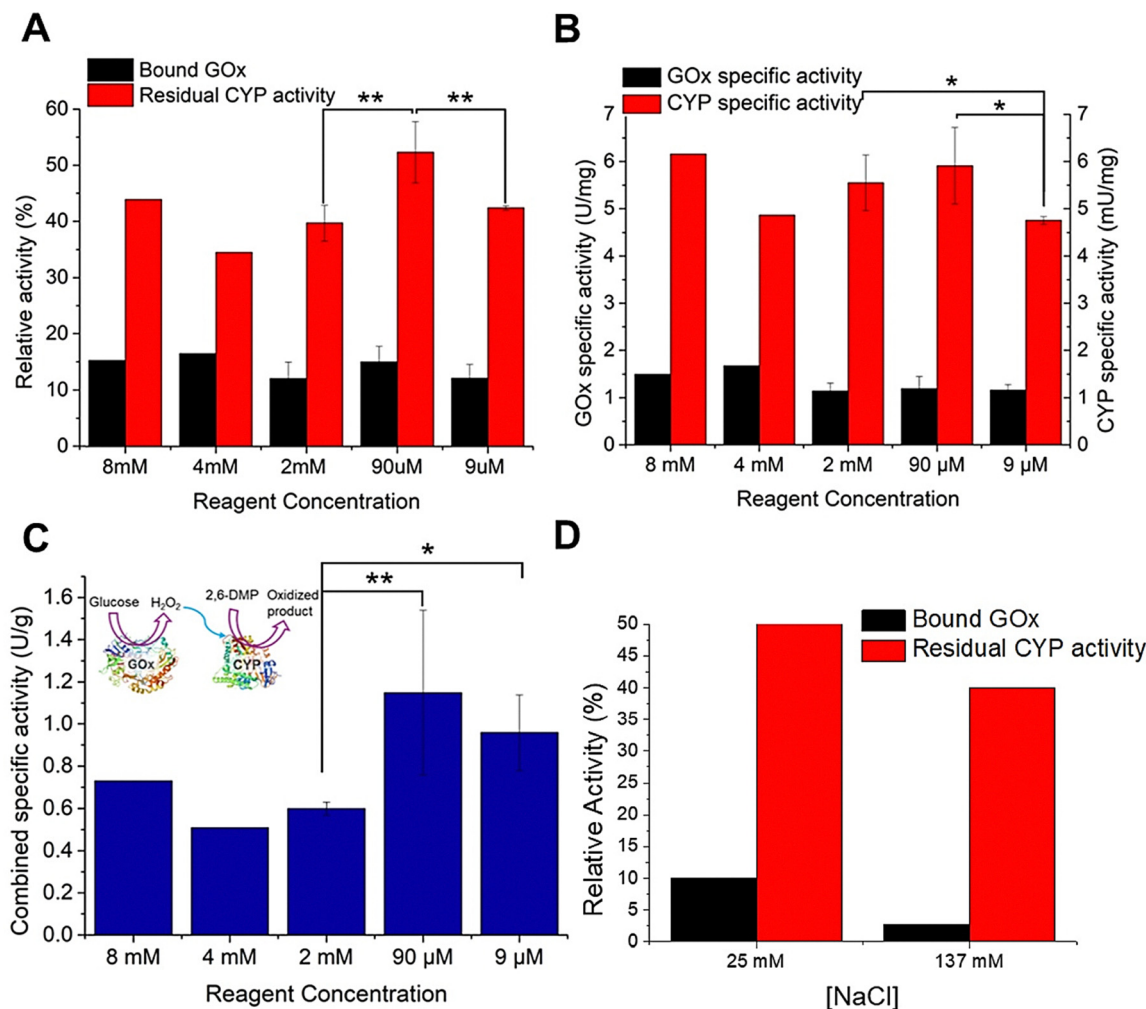
Fig. 4 Evaluation of multicomponent dual-enzyme nanoreactors functionalized *via* one-step Ugi reaction. (A) Relative surface-bound GOx and residual CYP activity across reagent concentrations. (B) Specific activity of surface-conjugated GOx and encapsulated CYP. (C) Overall cascade-specific activity using 2,6-DMP substrate. (D) Effect of ionic strength on residual enzyme activities. The results are presented as mean $\pm$ SD from five independent reactions. Statistical significance was determined using two-way ANOVA with Tukey's posttest (*$p < 0.05$, $p < 0.01$).

Cascade-specific activity was assessed by monitoring CYP-mediated substrate transformation in the presence of glucose. GOx oxidized glucose to gluconic acid while generating hydrogen peroxide *in situ*, which served as the final electron donor driving CYP catalysis. The highest activity (~ 1.4 mU mg^{-1}) was observed at 90 μM reagent concentration. Many chemotherapeutics are administered as prodrugs. Such cascade activity effectively mimics a glucose-responsive nanofactory, where in the glucose-rich tumor microenvironment (TME) the nanoreactors can drive CYP-mediated prodrug activation into cytotoxic metabolites, offering enhanced anticancer efficacy with reduced side effects.

All the above reactions were performed in PBS buffer with a 25 mM NaCl concentration. Further, the effect of high salt concentration for protein conjugation was also examined by comparing residual activity of the samples prepared at 25 mM and 137 mM NaCl in 50 mM PBS, and 90 μM reagent concentration. High ionic strength significantly reduced GOx retention (from $\sim 11\%$ to 2.7%) and slightly impacted CYP activity.

These results support the hypothesis that ionic shielding interferes with functionalization efficiency and possibly destabilizes non-covalent interactions critical for enzyme orientation on the capsid surface. At low ionic strength, electrostatic interactions between molecules become much stronger as fewer ions are in the solution to shield electrical charges. As a result, charged molecules can feel each other's presence over longer distances. This interparticle distance is the Debye length, which increases exponentially as ionic strength approaches zero.[31] Therefore, low ionic strength in the reaction medium increases the degree of reaction. Overall, the results show that the 90 μM condition offers the best compromise, ensuring high GOx activity, $> 50\%$ retained CYP functionality, and robust cascade performance.

After successful characterization of biochemical properties, the effect of reagent concentration on ICG conjugation was tested. Although ICG does not participate in the Ugi reaction due to the low nucleophilicity of its sulfonic acid groups, it binds non-covalently to the hydrophobic regions of the protein

Table 2 Influence of reagent concentrations on ICG binding through hydrophobic interactions. *Data are presented as mean ± SD from five independent reactions

Sample	ICG concentration ($\mu g\ mL^{-1}$)	μg of ICG per mg of protein
8 mM	11.65	5.32
4 mM	12.13	5.12
2 mM	9.46 ± 0.402	5.14 ± 0.091*
90 µM	10.53 ± 0.461	6.02 ± 0.072*
9 µM	8.11 ± 0.586	4.76 ± 0.172*

via hydrophobic stacking interactions. This interaction forms a biocompatible interface and reduces dye leakage, enhancing stability and biocompatibility.[32] ICG was used as an additional fluorescent component to track the *in vitro* localization of nanoreactors with the added advantage of phototherapy.

The extent of ICG binding to the VLP surface was quantified using a calibration curve. As shown in Table 2, ICG conjugation remained consistent across all tested reagent concentrations. This uniform binding profile indicates that the components involved in the Ugi reaction did not interfere with ICG attachment. Furthermore, the preservation of both ICG loading and GOx conjugation suggests that the Ugi reaction exhibits non-interfering and possibly site-selective behavior. The ICG stacking within hydrophobic domains of protein nanostructure remained unaffected, also indicating spatial compatibility of multiple components and the mildness of the Ugi reaction. Successful binding was also evident by the green pellet obtained after ultracentrifugation (Fig. 3a). Thus, ICG likely does not act as an active Ugi component but is co-immobilized within the multifunctional matrix.

The preservation of photoactivity of ICG was analyzed in final nanoreactors obtained at 90 µM reagent concentration. The absorption spectrum of ICG-labeled nanoreactors showed a characteristic absorbance peak of ICG near 780 nm, which was missing in the core P22CYP at similar concentrations (Fig. 5a). On the other hand, the additional absorption peak at the Soret region (~410 nm) corresponds to the heme group of CYP, further confirming the integrity of CYP.[33] The fluorescence of the nanoreactors was corroborated using a fluorescent blot imaging system. Excitation wavelengths were adjusted at 745–760 nm, and emission wavelengths were monitored at 810–850 nm. Positive control of ICG and negative controls containing P22-CYP and PBS buffer were used (Fig. 5b). At similar concentrations, the ICG-conjugated P22 exhibited stronger fluorescence than free ICG, suggesting reduced self-quenching due to spatial separation on the protein surface.

Fig. 5c illustrates the schematic for photoactivity assessment, where ICG-labeled nanoreactors in a 96-well plate were irradiated with 808 nm NIR light (0.5 W, 5 cm distance). Temperature changes of the nanoreactor solution (200 µL, 0.2 mg mL^{-1}) were recorded every 20 seconds for 5 minutes. Fig. 5d shows the cumulative temperature rise compared to controls. Upon NIR exposure, nanoreactors exhibited a noticeable temperature increase, confirming efficient photothermal conversion and retention of ICG's functional properties.

Photothermal therapy (PTT) involves converting NIR light into heat *via* photoabsorbers like ICG, inducing localized hyperthermia that damages cancer cell membranes. In this study, ICG raised the temperature by approximately 3.7 °C over 5 minutes. While other ICG-based nanocarriers under higher laser powers (1–1.5 W) report larger temperature increases, typically 15–20 °C within 2 minutes.[34–36] Therefore, the lower laser power (0.5 W) used here limits direct comparisons. Photothermal performance depends on multiple variables, including laser power density (W cm^{-2}) and nanocarrier type.

The generation of reactive oxygen species (ROS) by bound ICG was confirmed by qualitative monitoring of the change in fluorescence intensity of the ROS-sensitive dye, 1,3-diphenyl isobenzofuran (DPBF), after NIR irradiation. DPBF reacts with ROS and undergoes transformation to form non-fluorescent 1,2-dibenzoylbenzene (DBB). A decrease in the fluorescence of DPBF is related to an increase in the generation of singlet oxygen and superoxide radical.[37] The nanoreactors were mixed with DPBF (10 µM), the reaction mixture was irradiated with an 808 nm laser (0.5 W) in 2-minute intervals to determine the fluorescence using 410 nm as the excitation wavelength (Fig. 5e).

The time-dependent decrease in DPBF fluorescence under NIR light exposure confirmed the ability of nanoreactors to generate ROS, essential for photodynamic therapy (PDT). The decrease in fluorescence showed a first-order decay with pseudo-linear behavior between 0 to 4 minutes. After 6 minutes of irradiation, DPBF retained 50% of its initial fluorescence, and by the end of the experiment, about 35% of its fluorescence was retained. Overall, the analysis suggests the generation of ROS due to the excitation of ICG under NIR light, suggesting the preserved functional integrity of ICG under Ugi reaction conditions.

The catalytic performance of the bi-enzymatic nanoreactor was analyzed using a model enzymatic cascade reaction using 2,6-DMP as substrate and by varying the glucose concentration from 0 to 12 mM. As shown in Fig. 6A, the multifunctional P22CYP–GOx–GA–ICG nanoreactors enabled time-dependent oxidation of 2,6-DMP, indicating the successful cascade reaction, where GOx-generated hydrogen peroxide fuels the CYP450 catalytic cycle. As glucose concentrations are higher in tumor microenvironment, a self-activated prodrug transformation could be achieved specifically at the tumor region.[38]

Michaelis–Menten curves of the combined enzyme activity were processed to calculate the maximum velocity (V_{max}), the Michaelis–Menten constant (K_M), the turnover number (k_{cat}) of the nanoreactors, and the catalytic efficiency (k_{cat}/K_M). Cascade enzyme kinetics was systematically evaluated across the three synthesized nanoreactor variants: P22CYP–GOx (EDC–NHS) conjugated *via* carbodiimide coupling, P22CYP–GOx (Ugi) conjugated *via* Ugi, and the nanoreactor (P22CYP–GOx–GA–ICG) simultaneously functionalized with ICG and GA through Ugi. This comparison enabled a direct assessment of how the conjugation strategy and functionalization elements impacted the catalytic performance and efficiency of the whole system. The results are summarized in Table 3. Although P22CYP–GOx
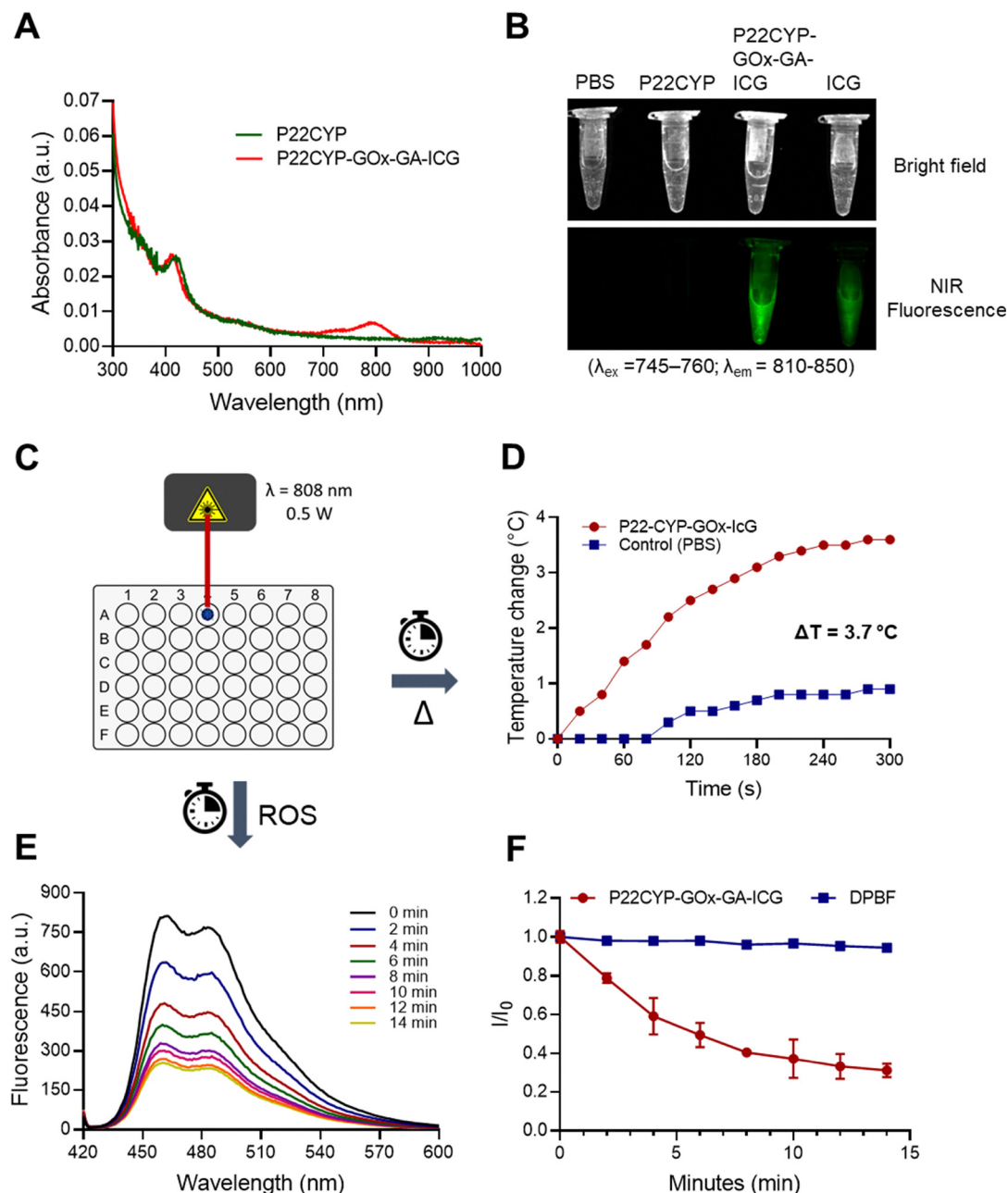
Fig. 5 Photochemical characterization of ICG-labeled P22 nanocages under NIR irradiation (808 nm). (A) UV-Vis absorption spectra confirming the presence of ICG in P22–ICG conjugates. (B) Fluorescence images of ICG-labeled samples under bright and NIR light compared to free ICG at similar concentrations. (C) Schematic representation of photothermal and photodynamic assays using 96-well plates. (D) Photothermal heating profile of PBS and ICG-bound nanoreactors over time upon NIR laser irradiation. (E) Fluorometric ROS production assay of the nanoreactors monitoring the change in the fluorescence intensity of DPBF after NIR irradiation. (F) Comparison of normalized decrease in DPBF fluorescence.

(EDC–NHS) has the highest k_{cat}, it also has the highest K_M, indicating lower substrate affinity. While both the UGI reaction involving only GOx (P22CYP–GOx) functionalization and multi-functionalization (P22CYP–GOx–GA–ICG) showed much stronger substrate affinity (K_M), resulting in the highest overall catalytic efficiency, making them efficient enzyme systems under lower substrate concentrations. However, the multifunctionalization resulted in a drop in k_{cat} while maintaining similar catalytic efficiency.

The biotransformation of tamoxifen, a model prodrug, using P22CYP–GOx–GA–ICG was also quantified by high-performance liquid chromatography (HPLC) under glucose-rich (25 mM) conditions to mimic a tumor-like microenvironment. The nanoreactors successfully transformed tamoxifen up to ∼43% *via* glucose-mediated cascade reaction (Fig. 6b). Upon exposure to NIR light (808 nm, 0.5 W), a significant increase in tamoxifen conversion was observed, reaching up to ∼70%. This enhancement highlights the contribution of the photoactivity of ICG
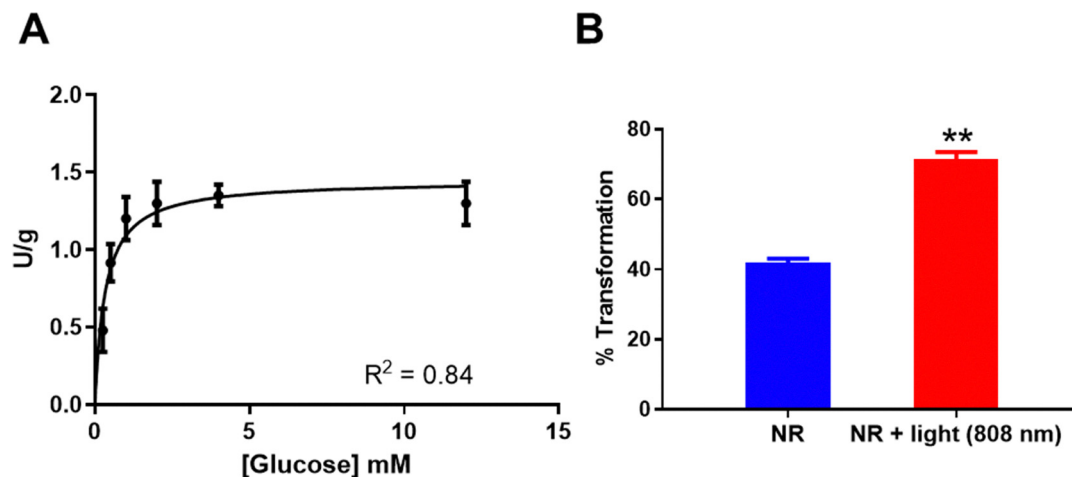
Fig. 6 Enzyme-catalyzed cascade reaction in the presence of glucose. (A) Transformation kinetics of 2,6-DMP using P22CYP–GOx–GA–ICG. (B) Quantification of tamoxifen biotransformation by HPLC showing increased conversion in the presence of NIR light (808 nm, 0.5 W) due to the synergistic effect of photodynamic and enzymatic prodrug activation. The results are expressed as the mean $\pm$ SD (n = 3). **p < 0.01 using an unpaired t-test.

Table 3 Enzyme kinetic constants for a cascade reaction

Nanoreactors	V_{max} (nmole min^{-1})	K_M (mM)	k_{cat} (min^{-1})	k_{cat}/K_M
P22CYP–GOx (EDC–NHS)	6.81	3.68	156.6	42.5
P22CYP–GOx (Ugi)	3.22	0.77	88	114.3
P22CYP–GOx–GA–ICG	1.45	0.3291	39.09	118.8

under light irradiation, which likely facilitates both increased local temperature and ROS, improving the enzymatic reaction.

The synergistic effect observed aligns with our previous findings, where the combination of photodynamic therapy (PDT) and enzyme-mediated prodrug activation amplified therapeutic outcomes.[16] In this system, ICG not only functions as a phototransducer but also potentiates biocatalytic reactions by promoting enzyme activity. Taken together, these results demonstrate that the integration of ICG, CYP, and GOx in a P22-based nanocarrier facilitates programmable drug biotransformation with light-controlled enhancement, offering a promising strategy for targeted and spatiotemporally regulated cancer theranostics.

Further, the cytotoxic potential of the P22CYP–GOx–GA–ICG nanoreactors was evaluated in MDA-MB-231 breast cancer cells under different glucose conditions to determine the role of glucosamine-mediated targeting. In the presence of glucose, P22CYP–GOx–GA–ICG nanoreactors induced significant cytotoxicity in both concentrations (Fig. 7a). At 25 μg mL^{-1} and 50 μg mL^{-1}, cell viability sharply dropped compared to
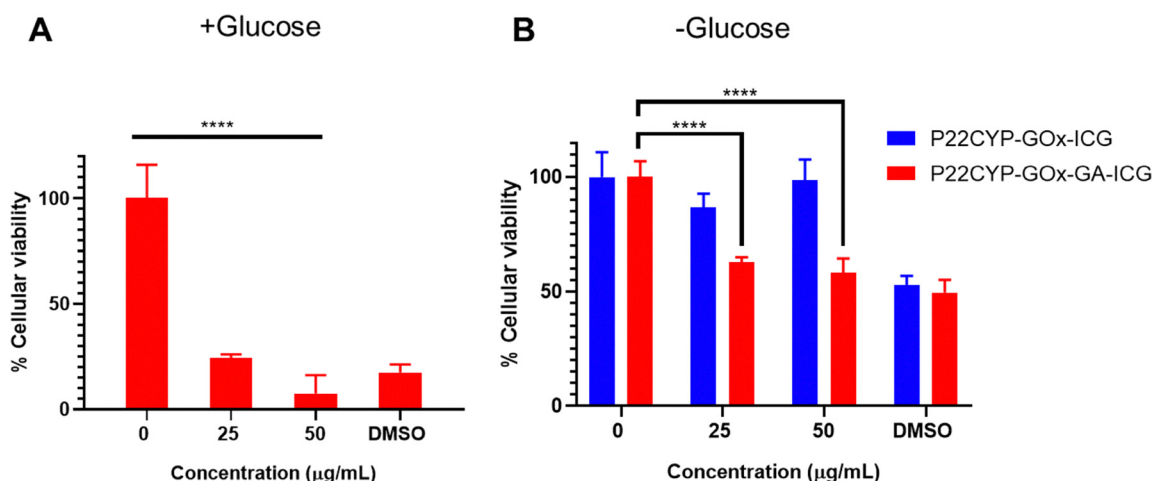

Fig. 7 In vitro cytotoxicity analysis of nanoreactors in MDA-MB-231 cells. (A) Cell viability after 12 h incubation with P22CYP–GOx–GA–ICG nanoreactors at increasing concentrations (0, 25, 50 μg mL^{-1}) in glucose-containing medium. (B) To assess glucosamine-mediated targeting, cells were first incubated with nanoreactors for 4 h in glucose-free medium to promote uptake, followed by washing, replacement with glucose-rich medium, and incubating for 12 h. P22CYP–GOx–GA–ICG nanoreactors (red bars) induced significantly greater cytotoxicity than P22CYP–GOx–ICG (blue bars). Data are shown as mean $\pm$ SD (n = 3). ****p < 0.0001 by unpaired t-test.
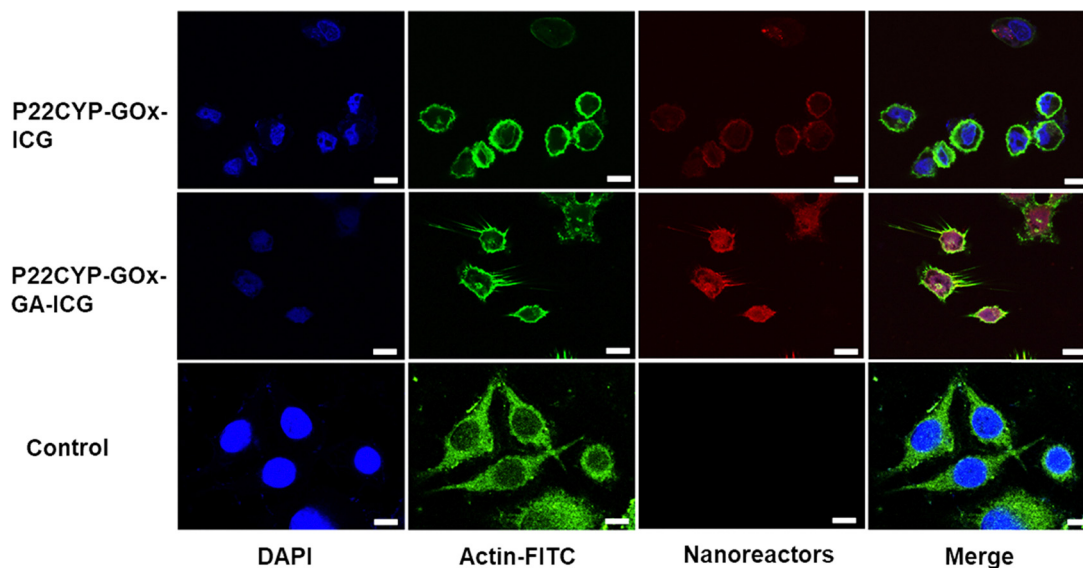
Fig. 8 Confocal fluorescence microscopy analysis of cellular internalization of nanoreactors in MDA-MB-231 cells. Cells were incubated for 4 hours in glucose-free medium with either P22CYP–GOx–ICG or glucosamine-functionalized P22CYP–GOx–GA–ICG nanoreactors. The nucleus was stained with DAPI (blue), actin cytoskeleton with actin-FITC (green), and nanoreactors visualized *via* ICG fluorescence (red). Scale bars: 10 μm.

untreated cells, suggesting that glucose oxidase (GOx) effectively catalyzed glucose oxidation, generating hydrogen peroxide and inducing oxidative stress. However, since glucose was abundantly available in the medium, the specific contribution of glucosamine targeting to cellular uptake could not be clearly distinguished in this condition, which is consistent with our previous findings.[19,39]

A modified protocol was employed to better assess the targeting role of glucosamine. Cells were incubated with nanoreactors in a glucose-free medium for 4 hours to encourage uptake *via* glucosamine-mediated endocytosis, followed by washing and re-introducing glucose-containing medium to trigger GOx activity intracellularly.

Under these conditions, a significant drop in viability was observed for P22CYP–GOx–GA–ICG-treated cells compared to control (Fig. 7b). While non-targeted nanoreactors did not show significant toxicity. This indicates enhanced uptake and intracellular GOx activity by glucosamine-modified nanoreactors. Similar cytotoxicity was observed in both 25 and 50 μg mL^{-1} concentrations, possibly reaching saturation in cell uptake in 4 h incubation. These findings clearly demonstrate the presence of glucosamine after multifunctionalization with the Ugi reaction. The non-toxicity of P22CYP–GOx–ICG also shows that the Ugi adducts are biocompatible in nature.

The internalization of nanoreactors in MDA-MB-231 cells was further investigated using confocal fluorescence microscopy. The cells were incubated with P22CYP–GOx–ICG and P22CYP–GOx–GA–ICG nanoreactors in glucose-free medium for 4 hours, followed by imaging. The nucleus was stained with DAPI (blue), the actin cytoskeleton with FITC (green), and ICG fluorescence from the nanoreactors was visualized in the red channel.

The cells treated with glucosamine-functionalized nanoreactors exhibited significantly higher red fluorescence intensity when compared to their non-targeted counterparts (Fig. 8). This clearly indicates enhanced cellular uptake facilitated by glucosamine, likely through interaction with overexpressed glucose transporters. In contrast, non-functionalized nanoreactors showed limited intracellular accumulation, as evidenced by weaker red signals.

Additionally, both nanoreactor-treated groups displayed morphological changes, which may indicate cellular stress induced by intracellular GOx activity of internalized nanoreactors. However, cytotoxicity analysis of non-targeted nanoreactors did not show any toxicity, indicating that replacement of the cell medium after 4 h restores cell viability (Fig. 7b). In confocal analysis, the cells were analyzed shortly after 4 h incubation to avoid possible cell death due to GOx activity in glucose rich medium. These findings strongly support the presence of glucosamine in improving internalization of targeted nanoreactor and suggest potential for enhanced therapeutic efficacy through controlled intracellular delivery.

3. Conclusion

The development of efficient, one-step methods for the multifunctionalization of nanocarriers remains a critical challenge in the design of advanced nanotherapeutics. This study is the first to successfully demonstrate the application of the Ugi four-component reaction on virus-like particles (VLPs), achieving multifunctionalization in a single step while preserving the structural integrity and functional properties of all incorporated moieties. Using P22CYP encapsulating cytochrome P450 (CYP), the reaction retained the enzymatic activity of the internalized CYP to a similar extent as observed with commonly applied carbodiimide coupling. P22CYP nanoreactors were

simultaneously functionalized with glucose oxidase (GOx) to drive cascade prodrug activation, glucosamine for targeted delivery, and indocyanine green (ICG) for both cellular tracking and phototoxic cancer therapy. This approach enabled TME responsive prodrug activation through enzyme cascade reaction, glucose-triggered oxidative stress, NIR-mediated photodynamic, and photothermal therapy for tumor.

In terms of cascade enzyme activity, carbodiimide coupled nanoreactors showed a higher turnover number, while the catalytic efficiency of Ugi produced nanoreactors was 2.7-fold improved. Importantly, this reaction did not interfere with ICG dye labeling, further highlighting its compatibility with parallel surface modifications. Interestingly, high reproducibility of reaction with consistent activities of GOx and CYP across varying reagent concentrations suggest potential selectivity of reaction, a feature previously observed primarily in antibodies.[12] Future studies probing site selectivity on complex VLP architectures will help establish precise functionalization strategies beyond genetic engineering. Overall, this work establishes Ugi-4CR as a powerful and versatile strategy for one-step multifunctionalization, advancing the modular design of VLP-based multimodal nanomedicines for cancer theranostics.

4. Materials and methods

4.1 Reagents

Glucose oxidase (GOx), hydrogen peroxide (0.6 M), formaldehyde (HCHO), *tert*-butyl isocyanide (*t*-BuNC), sodium chloride (NaCl), sucrose (glucose), glutaraldehyde, 1-ethyl-3-(3-dimethylaminopropyl)carbodiimide (EDC), N-hydroxysuccinimide (NHS), uranyl acetate, 2,6-dimethoxyphenol (DMP), horseradish peroxidase, guaiacol, 1,3-diphenylisobenzofuran (DPBF), indocyanide green (ICG), 2-glucosamine (GA), dimethylsulfoxide (DMSO) were purchased from the same producer (Sigma-Aldrich, St. Louis, MO). 1% agarose LE for superior separation of nucleic acids (Gold Biotechnology Inc, Olivette MO), jetBLUE (GeneDirex Inc, Taiwan), copper grids (400-mesh) coated with formvar/carbon support film (TedPel-la, USA), all other chemicals used were of highest grade commercially available.

4.2 Production and purification of P22CYP

4.2.1 Expression and purification of P22CYP VLPs and GOx preparation. The biocatalytic P22CYP VLPs were obtained as bacterial cell pellets produced from *E. coli* BL21(DE3) cells harboring the expression plasmids pBAD CYP-SP and pRSF P22 and purified *via* size exclusion chromatography as reported previously.[14] Commercial GOx from *Aspergillus niger* type II (Sigma-Aldrich, St. Louis, MO) was used for the multifunctionalization. The stock was prepared by dissolving GOx in 50 mM sodium acetate pH 5.1 to a working concentration of 5.46 mg mL^{-1} and later stored at −20 °C.

4.2.2 Quantification of P22CYP. Pierce BCA protein assay kit (Thermo Fisher Scientific) was used to quantify the amount of protein in the purified capsids solution. The assay is based on the interaction of protein with a reagent that leads to the reduction of Cu^{2+} to Cu^{+} under alkaline conditions, and the resultant complex shows absorption at 562 nm. Five different concentrations of the standard bovine serum albumin (BSA), and two different dilutions of the sample were tested in duplicate using the protocol given by the provider. After 30 min incubation of samples with the working reagent at 37 °C, the absorbance at 562 nm was measured using a UV-spectrometer (Multiskan GO, Thermo Scientific). The standard curve of BSA was plotted to estimate the concentration of P22 viral capsid in the samples.

4.2.3 Densitometric analysis on SDS-PAGE gel. Three different concentrations of purified P22, a non-purified sample of P22, and the sample corresponding to the aberrant VLPs were analyzed by electrophoresis. The samples were mixed with loading buffer in a 1 : 1 (v/v) ratio and heated at 95 °C for 10 minutes before running the gel. The samples were loaded, and the gel was run at 200 V for 1 : 30 hours. The gel was scanned in an SDS-PAGE gel transilluminator (iBright FL1000, Thermo Scientific). Finally, ImageJ software was used to perform the densitometric analysis and to estimate the ratio of CP and CYP-SP proteins.

4.2.4 Confinement molarity and percent occupancy. To calculate the confinement molarity and the percent occupation, eqn (1) and (2) were used, as described by Sharma *et al.*[40]

$$M = \frac{(N_{\text{enz}})}{(V_{\text{int}})(N_{\text{A}})} \quad (1)$$

Where M is the confinement molarity, N_{enz} is the number of CYP enzymes per capsid, V_{int} is the internal volume of the capsid, and N_{A} is the Avogadro number.

$$\%\text{Occupancy} = \frac{(N_{\text{enz}})(V_{\text{enz}})(100)}{(V_{\text{int}})} \quad (2)$$

Where N_{enz} is the number of CYP enzymes per capsid, V_{enz} is the volume of the CYP, and V_{int} is the internal volume of the capsid.

4.3 Bioconjugation of the nanoreactors

4.3.1 Glucose oxidase functionalization. Three different crosslinking reactions were tested to functionalize GOx from *Aspergillus niger* on the surface of the capsid. One reaction using glutaraldehyde, a second one using carbodiimide coupling with a combination of 1-ethyl-3-(3-dimethylaminopropyl)carbodiimide (EDC) and N-hydroxysuccinimide (NHS); and the third using the UGI-4CR reaction for dipeptide formation.

For the first reaction, GOx [125 µL (10.58 U mg^{-1}), 2 mg mL^{-1} stock] and P22CYP [250 µL (61.82 mU mg^{-1}), 1 mg mL^{-1} stock] were mixed in PBS buffer (pH 7.4) with glutaraldehyde [2 µL (∼2.6 µmol) of 12.5 wt% (∼1.29 M)] in a total reaction volume of 500 µL. The solution was left in constant agitation for 2 hours.

The second reaction consisted of two steps. Since GOx surface is rich with carboxylic acids,[39] the first step included the activation of carboxylic groups using EDC and NHS for 30 min in pH 6, followed by Amicon filtration to remove excess reagents. In the second step, the activated GOx was mixed with

P22CYP containing mild concentrations of EDC NHS at pH 7.4 to ensure the conjugation of proteins. Because the molecular weights of GOx (∼160 kDa) and P22 (∼27 MDa) differ by several orders of magnitude, careful optimization of reagent concentrations was essential. When the molar concentration of EDC/NHS was based on P22, it was insufficient to activate enough carboxyl groups on GOx for efficient coupling. Conversely, when calculated based on the molar amount of GOx, the excess cross-linker promoted nonspecific crosslinking and aggregation of P22. The two-step strategy therefore ensured efficient activation of GOx while minimizing P22 aggregation, leading to successful conjugation. Briefly, GOx [125 μL (10.58 U mg⁻¹), 2 mg mL⁻¹ stock] was mixed with 100 mole excess of EDC (∼30 μg) and NHS (∼18 μg) in a final volume of 250 μL and left under agitation for 30 minutes. It was centrifuged at 8000g (Multifuge X1R, Thermo Scientific) for 5 minutes in a 100 kDa Amicon filter to remove excess reagents. The activated GOx was mixed with the suspension of P22CYP [250 μL (61.82 mU mg⁻¹), 1 mg mL⁻¹ stock] containing 200 mole excess of EDC (0.35 μg) and NHS (∼0.21 μg). The final reaction mixture (500 μL) was left 2 h under constant agitation at room temperature.

Ugi reaction was performed as previously reported with slight modifications.[8] P22CYP [41.6 μL (61.82 mU mg⁻¹) from 6 mg mL⁻¹ stock] was mixed with formaldehyde (8 μL from 25 mM stock) and left for five minutes under agitation. Afterward, GOx [41.6 μl (10.58 U mg⁻¹) from 6 mg mL⁻¹] and t-BuNC (8 μL from 25 mM stock) were added to the mixture and left under agitation for 2 h at room temperature. The reaction was performed in a final volume of 100 μL where the final concentration of formaldehyde and t-BuNC was 2 mM.

After each reaction, amicon filtration was carried out using 100 kDa membrane filters to remove the excess reagents. The concentrate was resuspended to a final volume of 2.5 mL and ultracentrifuged using a fixed angle rotor 90 Ti (Optima XPN1000, Beckman Coulter) for 1:30 hours at 40 000 rpm, and 4 °C. The obtained pellets were resuspended in PBS buffer pH 7.4.

4.3.2 One-step multifunctionalization of P22CYP using Ugi reaction.

Multifunctionalization of P22-CYP VLPs was achieved in a single step using Ugi-4CR. To optimize the reaction conditions, five formulations were prepared using 1:1 molar ratio of formaldehyde and t-BuNC, at 8 mM, 4 mM, 2 mM, 90 μM, and 9 μM. Each sample contained same concentration of ICG, GA, P22CYP, and GOx in a final volume of 100 μL as shown in Table 4. The reaction was performed in phosphate buffer saline (PBS) (50 mM and 25 mM NaCl). The reaction was

initiated by pre-incubating P22-CYP VLPs with HCHO for 5 minutes at room temperature with gentle agitation. GOx, ICG, and GA were then sequentially added, followed by t-BuNC to initiate multicomponent coupling. The mixture was vortexed briefly to ensure homogenization and incubated under agitation for 2 hours at room temperature. After completion, the excess reagents were removed through amicon filtration using 100 kDa membrane filter. Subsequently, the green color pellet of VLPs was obtained via ultracentrifugation at 42 000 rpm for 1.5 hours using a 90 Ti rotor (Optima XPN 100, Beckman Coulter), and resuspended in 100 μL PBS. For reaction reproducibility, the reaction was repeated 5 times and both the post-reaction enzymatic activity of GOx and CYP and the degree of ICG conjugation was quantified as presented in Fig. 4(a)–(c) and Table 2, respectively.

To evaluate the effect of ionic strength on reaction efficiency, additional reactions at 2 mM reagent concentration were conducted in PBS supplemented with 25 mM or 132 mM NaCl.

4.4 Transmission electron microscope

Nanoreactors were analyzed using a transmission electron microscope (JEM-2010, JEOL). The voltage was set at 80 kV and the sample preparation was performed by staining the sample with 5 μL of 2% uranyl acetate for 2 min.

4.5 Enzyme activity of P22 nanoreactors

4.5.1 GOx activity analysis. The reaction medium was composed of sodium acetate buffer (50 mM, pH 5.1), dextrose (4.75 mM), and guaiacol (0.8 mM). To start the reaction, 957 μL of the reaction medium were mixed with 10 μL of the functionalized nanoreactors, and 33 μL of horseradish peroxidase (HRP) with an activity of 60 U mL⁻¹. The GOx undergoes glucose oxidation and produces H_2O_2 as a side product, which is used by HRP for guaiacol oxidation (ε_{470} = 26 600 M⁻¹ cm⁻¹).[17] The absorbance of oxidized guaiacol was monitored at 470 nm for 2 minutes using a UV-vis spectrometer (Lambda 25, PerkinElmer) to calculate the enzyme activity.

The determination of bound GOx percentage was calculated using eqn (1).

$$\%\text{Bound GOx} = \frac{\text{Activity of nanoreactors} \left(\text{U mg}^{-1}\right)}{\text{GOx activity used for synthesis} \left(\text{U mg}^{-1}\right)}$$

4.5.2 CYP activity analysis. The reaction medium for the CYP activity assay contained 2,6-dimethoxyphenol (DMP) (500 μM), and Tris-HCl buffer (pH 8, 50 mM). To start the

Table 4 Amounts of components used for the multifunctionalization of P22-CYP VLPs each reaction

HCHO and t-BuNC concentration (volume, stock)	P22-CYP VLP (μg) (activity, volume, stock)	GOx (μg) (activity, volume, stock)	IcG (μg) mole ratio [VLP:IcG]	GA (μg) mole ratio [VLP:2DG]	Total volume (μL)
8 mM (8 μL, 100 mM) 4 mM (4 μL, 100 mM) 2 mM (2 μL, 100 mM) 90 μM (9 μL, 1 mM) 9 μM (9 μL, 0.1 mM)	250 (11.5 mU mg⁻¹, 30.4 μL, 8.22 mg mL⁻¹)	250 (8.66 U mg⁻¹, 45.8 μL, 5.46 mg mL⁻¹)	4.68 [1:600]	1.89 [1:1200]	≈100

reaction, 985 μL of reaction medium were mixed with 10 μL of P22 nanoreactors, and H_2O_2 (5 mM) in a final volume of 1 mL. Immediately after the addition of hydrogen peroxide, the absorbance of the solution was monitored using a UV-spectrometer (Lambda 25, PerkinElmer) at 468 nm for 5 minutes. The molar extinction coefficient of the transformed product of DMP at 468 nm is 14 800 M^{-1} cm^{-1}.[17]

To determine the kinetic parameters of the cytochrome P450 in the P22-CYP nanoreactors, enzyme activity assays were performed with different concentrations of DMP. Obtained data was processed using GraphPad Prism 8.0.1 software to calculate the kinetic parameters.

The determination of CYP activity recovery in reactions was calculated using eqn (2).

$$\%CYP \text{ activity recovery} = \frac{\text{Activity of nanoreactors}\left(U\ mg^{-1}\right)}{\text{P22CYP activity used for synthesis}\left(U\ mg^{-1}\right)}$$

4.5.3 Combined activity assay. To measure the combined activity of CYP and GOx, the reaction medium contained Tris-HCl buffer (pH 8, 50 mM), DMP (500 μM), and glucose (95 μM). The medium (950 μL) was mixed with 33 μL of the functionalized nanoreactors (2 mg mL^{-1}), and the absorbance was monitored for 45 minutes at 468 nm using a UV-spectrometer (Lambda 25, PerkinElmer). The molar extinction coefficient of DMP transformation product at 468 nm is 14 800 M^{-1} cm^{-1}.[17]

The kinetic parameters of the GOx and CYP combined activity in cascade nanoreactors were determined. Different concentrations of glucose were used in enzyme assays, and the obtained data was processed using GraphPad Prism 8.0.1 software to calculate the kinetic parameters.

4.6 Biotransformation analysis of prodrug

The stock solution of tamoxifen was prepared in acetonitrile (ACN) at a concentration of 5 mM. For the biotransformation assay, the reaction mixture consisted of 500 μM tamoxifen and 50 mM PBS buffer (pH 7.4) in a final volume of 0.5 mL. Reactions were initiated by the addition of nanoreactors to achieve a final protein concentration of 50 μg mL^{-1}. For glucose-dependent activation, 100 μM glucose was included in the reaction mixture. Samples were incubated at 25 °C for 50 minutes either in the dark (no irradiation) or under near-infrared (NIR) light exposure. After incubation, the reaction mixture was centrifuged at 13 000 rpm for 5 minutes to remove particulate matter before analysis.

High-performance liquid chromatography (HPLC) was performed using an Agilent 1100 series system equipped with an Ascentis C18 reverse-phase column (Supelco, 150 × 4.6 mm, 3 μm). Samples were injected into the column and eluted isocratically at a flow rate of 1 mL min^{-1} using a mobile phase composed of 30% water (A) and 70% ACN (B), both containing 0.1% trifluoroacetic acid (TFA). Elution was monitored at 280 nm. All solvents were filtered through a 0.22 μm nylon membrane before use. The extent of tamoxifen biotransformation was quantified by calculating the percentage decrease in the area under the tamoxifen peak relative to the control sample.

4.7 Characterization of bound ICG

4.7.1 Quantification of ICG on the nanoreactors. Five different concentrations (0.1 to 0.5 μg mL^{-1}) of ICG diluted in PBS buffer were used to obtain a calibration curve; the maximum absorbance at 790 nm of the solutions was measured using a UV-vis spectrometer (Lambda 25, PerkinElmer). The same absorbance was measured in a diluted concentration of the nanoreactors to estimate the concentration of bound ICG.

4.7.2 Absorption and fluorescence of the nanoreactors. A fluorescent blot imaging system (iBright FL1000, Thermo Fisher Scientific) was used to observe the fluorescence of the nanoreactor after the functionalization of ICG. Excitation and emission wavelengths were adjusted to 745–760 and 810–850 nm respectively. Eppendorf tubes with PBS buffer, P22CYP, and P22CYP–GOx–GA–ICG nanoreactors were scanned with an exposure time of 1326 ms.

The absorption spectrum of the nanoreactors in each functionalization step was obtained using a UV-spectrometer (Lambda 25, PerkinElmer), the absorbance was measured from 300 to 1000 nm with the same concentration of protein in all samples.

4.7.3 Analysis of reactive oxygen species. The ROS generation assay was performed by monitoring the degradation of 1,3-diphenylisobenzofuran (DPBF) in a fluorescence spectrophotometer (Cary Eclipse, Agilent Technologies). For the assay, 20 μg of the ICG-functionalized nanoreactors (0.12 μg of ICG) were mixed with DPBF (10 μM) and DMSO (10%) in a final volume of 200 μL. This solution was irradiated with an 808 nm laser (0.5 W) in intervals of two minutes for a total exposure time of 12 minutes; after each interval, the emission fluorescence spectrum was obtained using 410 nm as the excitation wavelength.

4.7.4 Thermal properties. The change in the temperature of the nanoreactors under near-infrared light was monitored using a digital source (FOB100, Omega) coupled to an optical fiber temperature sensor. 180 μg of ICG-functionalized nanoreactors (equivalent to 1.08 μg of ICG) were diluted in 100 μL of PBS buffer and irradiated with an 808 nm laser (0.5 W) for 5 minutes, the temperature of the nanoreactors was measured in 20 seconds intervals. PBS buffer was used as a control for this analysis.

4.8 In vitro cells analysis

4.8.1 MTT cytotoxicity assay. MDA-MB-231 cells at 80% confluence were washed with 1× PBS, detached using trypsin/EDTA, and resuspended in complete DMEM supplemented with 10% FBS and 1% antibiotic–antimycotic. A total of 1 × 10^4 cells per well were seeded into 96-well plates and incubated overnight at 37 °C in a 5% CO_2 atmosphere.

The next day, cells were washed with 1× PBS and treated with nanoreactor suspensions under two distinct conditions:

• Condition 1 – continuous glucose exposure (12 h treatment): nanoreactors were resuspended in DMEM containing

glucose and added directly to the cells, followed by incubation for 12 h at 37 °C and 5% CO_2.

• Condition 2 – glucose-free preincubation (4 h uptake + 12 h treatment): nanoreactors were resuspended in glucose-free DMEM and added to cells for a 4 h incubation to promote internalization. Following this, cells were washed with 1× PBS and replenished with complete DMEM (with glucose) and incubated for 12 h.

Thereafter, cells were washed with 1× PBS and incubated with MTT solution (10% v/v in DMEM) for 4 h at 37 °C and 5% CO_2. After incubation, MTT solvent was added, and the plates were incubated for an additional 12 h to dissolve formazan crystals. Absorbance was measured at 570 nm using a microplate reader to evaluate cell viability.

4.8.2 Cellular internalization by confocal imaging. MDA-MB-231 cells (5×10^4) were seeded onto poly-L-lysine-coated glass coverslips and incubated for 12 h at 37 °C in a 5% CO_2 humidified incubator using complete high-glucose DMEM. After incubation, cells were gently washed twice with 1× PBS, and nanoreactors (25 µg mL^{-1}) were added in glucose-free DMEM. The cells were then incubated for 4 h under the same conditions to allow internalization. Following treatment, cells were fixed with 4% paraformaldehyde at 4 °C for 30 minutes and washed three times with 1× PBS. Permeabilization was performed using 0.3% Tween-20 in 1× PBS for 20 minutes at room temperature. To prevent non-specific binding, cells were blocked with 2% bovine serum albumin (BSA) in 1× PBS for 1 hour at 37 °C.

Subsequently, cells were incubated with anti-actin IgG conjugated with FITC for 1 hour at 37 °C, followed by two washes with 1× PBS. Cell nuclei were stained with 0.5 ng mL^{-1} DAPI (4′,6-diamidino-2-phenylindole) for 10 minutes in the dark at room temperature and rinsed twice with 1× PBS. Coverslips were then mounted and visualized using an Olympus Fluoview FV-1000 inverted laser-scanning confocal microscope. The emission of nanoreactors was analyzed in red channel with $\lambda_{excitation}$ = 635 nm and $\lambda_{emission}$ = 664 nm.

Conflicts of interest

Authors declare no conflicts of interest.

Data availability

The supplementary information contains protocol for P22CYP purification, characterization and enzyme kinetics analysis of encapsulated CYP. See DOI: **https://doi.org/10.1039/d5ma00416k**.

The data that support the findings of this study are available from the corresponding author upon reasonable request.

Acknowledgements

References

1 World Health Organization, "Cancer." Accessed: May 15, 2023. [Online]. Available: **https://www.who.int/news-room/fact-sheets/detail/cancer**.

2 A. S. Cleary, T. L. Leonard, S. A. Gestl and E. J. Gunther, Tumour cell heterogeneity maintained by cooperating sub-clones in Wnt-driven mammary cancers, *Nature*, 2014, **508**(7494), 113–117, DOI: **10.1038/nature13187**.

3 W. Fan, B. Yung, P. Huang and X. Chen, Nanotechnology for Multimodal Synergistic Cancer Therapy, *Chem. Rev.*, 2017, **117**(22), 13566–13638, DOI: **10.1021/acs.chemrev.7b00258**.

4 J. Shi, P. W. Kantoff, R. Wooster and O. C. Farokhzad, Cancer nanomedicine: progress, challenges and opportunities, *Nat. Rev. Cancer*, 2017, **17**(1), 20–37, DOI: **10.1038/nrc.2016.108**.

5 R. Van Der Meel, E. Sulheim, Y. Shi, F. Kiessling, W. J. M. Mulder and T. Lammers, Smart cancer nanomedicine, *Nat. Nanotechnol.*, 2019, **14**(11), 1007–1017, DOI: **10.1038/s41565-019-0567-y**.

6 J. L. Mejía-Méndez, R. Vazquez-Duhalt, L. R. Hernández, E. Sánchez-Arreola and H. Bach, Virus-like Particles: Fundamentals and Biomedical Applications, *Int. J. Mol. Sci.*, 2022, **23**(15), 8579, DOI: **10.3390/ijms23158579**.

7 O. González-Davis, M. V. Villagrana-Escareño, M. A. Trujillo, P. Gama, K. Chauhan and R. Vazquez-Duhalt, Virus-like nanoparticles as enzyme carriers for Enzyme Replacement Therapy (ERT), *Virology*, 2023, **580**, 73–87, DOI: **10.1016/j.virol.2023.01.017**.

8 S. Rezaei, A. Landarani-Isfahani, M. Moghadam, S. Tangestaninejad, V. Mirkhani and I. Mohammadpoor-Baltork, Development of a novel bi-enzymatic silver dendritic hierarchical nanostructure cascade catalytic system for efficient conversion of starch into gluconic acid, *Chem. Eng. J.*, 2019, **356**, 423–435, DOI: **10.1016/j.cej.2018.09.046**.

9 S. E. Hooshmand and W. Zhang, Ugi Four-Component Reactions Using Alternative Reactants, *Molecules*, 2023, **28**(4), 1642, DOI: **10.3390/molecules28041642**.

10 R. O. Rocha, M. O. Rodrigues and B. A. D. Neto, Review on the Ugi Multicomponent Reaction Mechanism and the Use of Fluorescent Derivatives as Functional Chromophores, *ACS Omega*, 2020, **5**(2), 972–979, DOI: **10.1021/acsomega.9b03684**.

11 I. Ugi, R. Meyr, U. Fetzer and C. Steinbrück-ner, *Angew. Chem.*, 1959, **71**, 386, DOI: **10.1002/ange.19590711110**.

12 C. Sornay, *et al.*, Investigating Ugi/Passerini Multicomponent Reactions for the Site-Selective Conjugation of Native Trastuzumab, *Chem. – Eur. J.*, 2020, **26**(61), 13797–13805, DOI: **10.1002/chem.202002432**.

13 L. Sánchez-Sánchez, et al., Chemotherapy pro-drug activation by biocatalytic virus-like nanoparticles containing cytochrome P450, Enzyme Microb. Technol., 2014, 60, 24–31, DOI: 10.1016/j.enzmictec.2014.04.003.

14 L. Sánchez-Sánchez, et al., Design of a VLP-nanovehicle for CYP450 enzymatic activity delivery, J. Nanobiotechnol., 2015, 13(1), 66, DOI: 10.1186/s12951-015-0127-z.

15 A. Tapia-Moreno, K. Juarez-Moreno, O. Gonzalez-Davis, R. D. Cadena-Nava and R. Vazquez-Duhalt, Biocatalytic virus capsid as nanovehicle for enzymatic activation of Tamoxifen in tumor cells, Biotechnol. J., 2017, 12(6), 1600706, DOI: 10.1002/biot.201600706.

16 K. Chauhan, J. M. Hernandez-Meza, A. G. Rodríguez-Hernández, K. Juarez-Moreno, P. Sengar and R. Vazquez-Duhalt, Multifunctionalized biocatalytic P22 nanoreactor for combinatory treatment of ER+ breast cancer, J. Nanobiotechnol., 2018, 16(1), 17, DOI: 10.1186/s12951-018-0345-2.

17 O. González-Davis, K. Chauhan, S.-J. Zapian-Merino and R. Vazquez-Duhalt, Bi-enzymatic virus-like bionanoreactors for the transformation of endocrine disruptor compounds, Int. J. Biol. Macromol., 2020, 146, 415–421, DOI: 10.1016/j.ijbiomac.2019.12.272.

18 L. P. Sánchez and R. Vázquez-Duhalt, Cápsides virales como nanoacarreadores enzimáticos para quimioterapia, 1 de agosto de, 2014, vol. 15, no. 8, [Online], Available: https://www.revista.unam.mx/vol15/num8/art61/index.html.

19 K. Chauhan, P. Sengar, K. Juarez-Moreno, G. A. Hirata and R. Vazquez-Duhalt, Camouflaged, activatable and therapeutic tandem bionanoreactors for breast cancer theranosis, J. Colloid Interface Sci., 2020, 580, 365–376, DOI: 10.1016/j.jcis.2020.07.043.

20 O. González-Davis, C. Kanchan and R. Vazquez-Duhalt, Biocatalytic Nanoreactors for Medical Purposes, Pharmaceutical Biocatalysis, Jenny Stanford Publishing, 2019.

21 K. E. Sapsford, et al., Functionalizing Nanoparticles with Biological Molecules: Developing Chemistries that Facilitate Nanotechnology, Chem. Rev., 2013, 113(3), 1904–2074, DOI: 10.1021/cr300143v.

22 A. Zlotnick, M. M. Suhanovsky and C. M. Teschke, The energetic contributions of scaffolding and coat proteins to the assembly of bacteriophage procapsids, Virology, 2012, 428(1), 64–69, DOI: 10.1016/j.virol.2012.03.017.

23 I. Migneault, C. Dartiguenave, M. J. Bertrand and K. C. Waldron, Glutaraldehyde: Behavior in Aqueous Solution, Reaction with Proteins, and Application to Enzyme Cross-linking, Biotechniques, 2004, 37(5), 790–802, DOI: 10.2144/04375RV01.

24 I. Matijošytė, I. W. C. E. Arends, S. de Vries and R. A. Sheldon, Preparation and use of cross-linked enzyme aggregates (CLEAs) of laccases, J. Mol. Catal. B: Enzym., 2010, 62(2), 142–148, DOI: 10.1016/j.molcatb.2009.09.019.

25 V. V. Kumar, S. Sivanesan and H. Cabana, Magnetic cross-linked laccase aggregates—Bioremediation tool for decolorization of distinct classes of recalcitrant dyes, Sci. Total Environ., 2014, 487, 830–839, DOI: 10.1016/j.scitotenv.2014.04.009.

26 L. K. Escalante Morales, P. Sengar, A. Dorado Baeza, R. Vazquez-Duhalt and K. Chauhan, Enhanced Laccase Activity and Stability as Crosslinked Enzyme Aggregates on Magnetic Copper Ferrite Nanoparticles for Biotechnological Processes, ChemCatChem, 2023, 15(22), e202301071, DOI: 10.1002/cctc.202301071.

27 G. Pastuch-Gawołek, J. Szreder, M. Domińska, M. Pielok, P. Cichy and M. Grymel, A Small Sugar Molecule with Huge Potential in Targeted Cancer Therapy, Pharmaceutics, 2023, 15(3), 913, DOI: 10.3390/pharmaceutics15030913.

28 J. H. Quastel and A. Cantero, Inhibition of Tumour Growth by D-Glucosamine, Nature, 1953, 171(4345), 252–254, DOI: 10.1038/171252a0.

29 C.-H. Lu and J.-K. Hsiao, Indocyanine green: An old drug with novel applications, Tzu Chi Med. J., 2021, 33(4), 317, DOI: 10.4103/tcmj.tcmj_216_20.

30 C. Shirata, et al., Near-infrared photothermal/photodynamic therapy with indocyanine green induces apoptosis of hepatocellular carcinoma cells through oxidative stress, Sci. Rep., 2017, 7(1), 13958, DOI: 10.1038/s41598-017-14401-0.

31 C. Park and R. T. Raines, Quantitative Analysis of the Effect of Salt Concentration on Enzymatic Catalysis, J. Am. Chem. Soc., 2001, 123(46), 11472–11479, DOI: 10.1021/ja0164834.

32 Z.-Y. Dai, C. Shen, X.-Q. Mi and Q. Pu, The primary application of indocyanine green fluorescence imaging in surgical oncology, Front. Surg., 2023, 10, 1077492, DOI: 10.3389/fsurg.2023.1077492.

33 A. Luthra, I. G. Denisov and S. G. Sligar, Spectroscopic features of cytochrome P450 reaction intermediates, Arch. Biochem. Biophys., 2011, 507(1), 26–35, DOI: 10.1016/j.abb.2010.12.008.

34 W. Shan, et al., Improved Stable Indocyanine Green (ICG)-Mediated Cancer Optotheranostics with Naturalized Hepatitis B Core Particles, Adv. Mater., 2018, 30(28), 1707567, DOI: 10.1002/adma.201707567.

35 Z. Wan, et al., Highly Efficient Hierarchical Micelles Integrating Photothermal Therapy and Singlet Oxygen-Synergized Chemotherapy for Cancer Eradication, Theranostics, 2014, 4(4), 399–411, DOI: 10.7150/thno.8171.

36 S. Long, et al., Characteristics of temperature changes in photothermal therapy induced by combined application of indocyanine green and laser, Oncol. Lett., 2019, 17(4), 3952–3959, DOI: 10.3892/ol.2019.10058.

37 P. Sengar, et al., Development of a functionalized UV-emitting nanocomposite for the treatment of cancer using indirect photodynamic therapy, J. Nanobiotechnol., 2018, 16(1), 19, DOI: 10.1186/s12951-018-0344-3.

38 L. Szablewski, Expression of glucose transporters in cancers, Biochim. Biophys. Acta, Rev. Cancer, 2013, 1835(2), 164–169, DOI: 10.1016/j.bbcan.2012.12.004.

39 P. Gama, P. Juárez, A. G. Rodríguez-Hernández and R. Vazquez-Duhalt, Glucose oxidase virus-based nanoreactors for smart breast cancer therapy, Biotechnol. J., 2023, 18(10), 2300199, DOI: 10.1002/biot.202300199.

40 J. Sharma and T. Douglas, Tuning the catalytic properties of P22 nanoreactors through compositional control, Nanoscale, 2019, 12(1), 336–346, DOI: 10.1039/C9NR08348K.